Photodissociation of H_2^+ and HD^+ in an intense laser field

A. Kondorskiy* and H. Nakamura†

Department of Theoretical Studies, Institute for Molecular Science, Myodaiji, Okazaki 444-8585, Japan

The photodissociation of H_2^+ and HD^+ by an intense laser pulse is investigated by solving the close-coupling equations without discretization. For the case of H_2^+ the photodissociation spectra are calculated under the condition mimicking the experimental one, and a fairly good agreement with the experiment is obtained. The uncertainty in the relative phases of initial states is found to lead to somewhat smoothing of the spectra, depending on the pulse length. It is also found that Raman-type transitions via intermediate dissociation continuum play an important role in determining the photodissociation spectra. This leads to a population increase of lower vibrational states and deforms the spectral profile. Dissociation from the lower vibrational states due to the bond softening is not strong enough. Photodissociation spectra and angular distribution are calculated also for HD^+ under the same conditions as in the H_2^+ case. The dipole transitions lead to additional structures in the energy spectra and angular distribution. There is a noticeable difference in the peak positions of dissociation spectrum for particles dissociated by the direct electronic-dipole transition and by the transitions via intermediate bound states. The photodissociation dynamics is further clarified by using the three-dimensional plots of the spectra as a function of the field intensity and frequency.

I. INTRODUCTION

Interactions of molecules with intense electromagnetic fields are a subject of wide interest and active research, recently. Such phenomena as the above threshold ionization and above threshold dissociation [1,2], bond softening [3,4], and bond hardening [5,6] have been actively investigated in the last decade. Significant theoretical interest in these subjects has been focused on the one-electron molecules H_2^+ and HD^+ because of their relative simplicity. Since the first two electronic states are energetically well separated from the higher states, the number of states involved in the processes is not large. It is possible to propose physical pictures of the processes listed above. These molecules represent fundamental diatomic molecules, homonuclear and heteronuclear, and exhibit different features in an intense electromagnetic field [7,8].

In the past few years, the experimental technique has been progressed quite a lot and made it possible to experimentally clarify the photodissociation dynamics of H_2^+ and HD^+ in an intense laser field [9–12]. One of the main problems in the experiment, however, has been the concern about the initial vibrational state distributions of target ions [13]. In early experiments, the same laser pulse was used to produce the target molecular ions via multiphoton ionization of neutral precursors and to photodissociate the target ions. This caused the initial-state distribution unknown, and made the analysis complicated because of the presence of neutral precursors. Recently, this uncertainty has been removed [10] by producing ions by dc electric discharge and the initial rovi-

brational state distribution has been determined relatively accurately. Assuming this state distribution, some experimental and theoretical works have been carried out [14–16].

However, the initial condition still causes a difficulty for a quantitative comparison between experiment and theory. This difficulty concerns about the relative phases of the initial amplitudes, which cannot be known and should inevitably be averaged. Besides, it is crucial to take into account a large number of bound states, which causes additional difficulty for quantitative theoretical studies.

The aim of this paper is to apply the recently developed effective method to studying the dissociation dynamics of H_2^+ and HD^+ in an intense laser field under the conditions that mimic the experimental ones. The theoretical approach used here is the close-coupling method based on the time-dependent integral equations (TIE) without any discretization of the continuum. This has been successfully applied to the ionization of atoms [17,18].

It will be demonstrated that various multistep transitions play crucial roles to determine the energy and angular distributions in the photodissociation. These transitions include dissociations via various intermediate discrete states and Raman-type transitions via the continuum and are rather sensitive to the laser parameters.

The organization of this paper is as follows: in the next section, the approach recently developed for atoms [17,18] based on the properties of TIE is reformulated so as to deal with the molecular target. In Sec. III, comparisons between our calculations and experiment [10] for the case of H_2^+ are presented. Effects of initial phase and population as well as a role of Raman-type transitions are discussed. Additional processes that play crucial roles in the case of HD^+ are discussed in Sec IV. A brief summary is presented in Sec. V.

---

*Permanent address: Lebedev Physical Institute, Leninsky pr., 53, Moscow 119991, Russia.

†Also at Department of Functional Molecular Science, The Graduate University for Advanced Studies, Myodaiji, Okazaki 444-8585, Japan.

II. CLOSE COUPLING APPROACH

A. Basic equations

The time-dependent Schrödinger equation for a molecular system interacting with an external laser field is written as

$$\left[i\frac{\partial}{\partial t} - \hat{H}_0(\mathbf{R},\mathbf{r}) - (\mathbf{d_r}+\mathbf{d_R})\cdot\mathbf{F}(t) \right]\Psi(\mathbf{R},\mathbf{r},t)=0, \quad (1)$$

where $\hat{H}_0(\mathbf{R},\mathbf{r})$ is the unperturbed Hamiltonian of the molecular system, $\mathbf{d_r}$ and $\mathbf{d_R}$ are the total electronic and nuclear dipole moment, and $\mathbf{F}(t)$ is a time-dependent external field, which is supposed to be a linearly polarized femtosecond pulse with a Gaussian profile. As usual, $\mathbf{r}$ and $\mathbf{R}$ stand for electron and nuclear coordinate vector, respectively.

We employ the close-coupling method on the basis of the discrete and continuum eigenfunctions of unperturbed Hamiltonian, $\hat{H}_0(\mathbf{R},\mathbf{r})$, under the Born-Oppenheimer approximation and expand the total wave function as

$$\Psi(\mathbf{R},\mathbf{r},t)=\sum_{n,v,K} a_{nvK}(t)\psi_n(\mathbf{R},\mathbf{r})\theta_{nvK}(\mathbf{R})e^{-iE_{nvK}\cdot t}$$

$$+\sum_{n,K}\int b_{n\mathbf{q}K}(t)\psi_n(R,r)\theta_{n\mathbf{q}K}(\mathbf{R})e^{-iE_{nqK}\cdot t}d\mathbf{q},$$

$$(2)$$

where n is the index to represent electronic bound state, v and $\mathbf{q}$ are the similar indices for nuclear motion, v for vibration and $\mathbf{q}$ for the momentum of dissociation continuum, and K is the rotational quantum number. The functions $\psi_{\mathbf{p}}(\mathbf{R},\mathbf{r})$ and $\theta_{n\{v\}K}(\mathbf{R})$ are the corresponding electronic and nuclear stationary-state wave functions, E_{nvK} are the energies of the discrete states, $E_{nqK}=q^2/2$ is the energy of the continuum state, and $a_{nvK}(t)$ and $b_{n\mathbf{q}K}(t)$ are the unknown coefficients. Atomic units are employed throughout the paper, unless otherwise noted.

Potential-energy curves of the ground and first three excited electronic states of H_2^+ molecule are presented in Fig. 1. In the case of external field, with wavelength about 785 nm (≈ 1.6 eV) used in most of the experiments, the energy difference between the first and second excited potential-energy curves is not smaller than the energy of four photons. Thus the attractive ground state, $1s\sigma_g$, and the first excited repulsive state, $2p\sigma_u$, are good enough to be considered in Eq. (2). The Hermitian system of coupled equations for the coefficients $a_{nvK}(t)$ for the discrete states and $b_{n\mathbf{q}K}(t)$ for the dissociation continuum follow from substituting the expansion (2) into Eq. (1) as

$$i\frac{da_{nvK}(t)}{dt}=\sum_{n',v',K'}\mathbf{U}_{nvK,n'v'K'}(t)a_{n'v'K'}(t)$$

$$+\sum_{n',K'}\int \mathbf{U}_{nvK,n'\mathbf{q}K'}(t)b_{n'\mathbf{q}K'}(t)d\mathbf{q} \quad (3)$$

and

$$i\frac{db_{n\mathbf{q}K}(t)}{dt}=\sum_{n',v',K'}\mathbf{U}_{n\mathbf{q}K,n'v'K'}(t)a_{n'v'K'}(t)$$

$$+\sum_{n',K'}\int \mathbf{U}_{n\mathbf{q}K,n'\mathbf{q}'K'}(t)b_{n'\mathbf{q}'K'}(t)d\mathbf{q}', \quad (4)$$
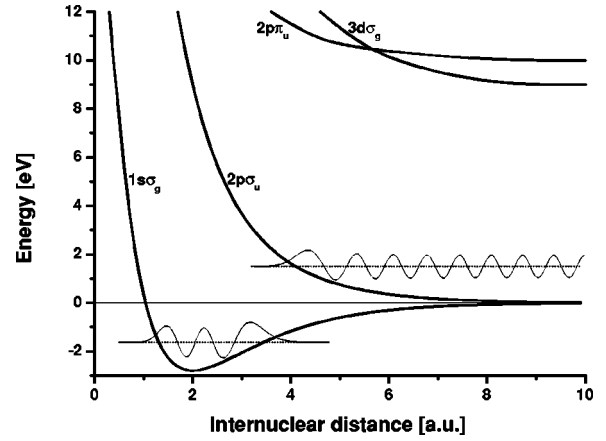

FIG. 1. Potential-energy curves for the ground and first three excited electronic states of H_2^+ together with schematic radial wave functions of bound and free states.

with

$$\mathbf{U}_{n\{v\mathbf{q}\}K,n'\{v'\mathbf{q}'\}K'}(t)=\mathbf{F}(t)\cdot\langle\theta_{n\{v\mathbf{q}\}K}(\mathbf{R})e^{iE_{n\{v\mathbf{q}\}K}\cdot t}|\mathbf{d}_{n,n'}^{(e)}(\mathbf{R})$$

$$+\mathbf{d}^{(N)}(\mathbf{R})|\theta_{n'\{v'\mathbf{q}'\}K'}$$

$$\times(\mathbf{R})e^{-iE_{n'\{v'\mathbf{q}'\}K'}\cdot t}\rangle, \quad (5)$$

$$\mathbf{d}_{n,n'}^{(e)}(\mathbf{R})=\langle\psi_n(\mathbf{R},\mathbf{r})|\mathbf{d_r}|\psi_{n'}(\mathbf{R},\mathbf{r})\rangle,$$

$$\mathbf{d}^{(N)}(\mathbf{R})=-\frac{e}{2}\frac{M_0-M_1}{M_0+M_1+m}\mathbf{R}, \quad (6)$$

where M_0 and M_1 are the masses of the nucleus ($M_0 > M_1$), m is the mass of electron, and e is its charge. The first and second terms in Eq. (3) describe the bound-bound and free-bound transitions, respectively. In Eq. (4), the first sum describes dissociation from all the discrete nuclear states and the integral term (free-free transitions) corresponds to nuclear scattering process. In Eqs. (3)–(6), the basis wave functions are obtained from numerical solutions of the radial Schrödinger equation with the potential-energy curves of $1s\sigma_g$ and $2p\sigma_u$ taken from [19,20] and the electronic transition dipole momentum from Refs. [20,21].

The nuclear symmetry or asymmetry in H_2^+ and HD^+ naturally causes differences in transitions and structures of Eqs. (3) and (4). Since the electronic transition dipole moment, $\mathbf{d}_{n,n'}^{(e)}(\mathbf{R})$, couples the two electronic states, $1s\sigma_g$ and $2p\sigma_u$, the nuclear transitions are possible only for bound-free and free-free for the same nuclear rotational quantum number K. Contrary to this, the nuclear dipole moment which is zero in the case of H_2^+ couples the states with different K under the selection rule $\Delta K=\pm 1$. This can induce bound-bound, bound-free and free-free transitions within the same electronic state. Thus, naturally, the case of HD^+ is more complicated with the nuclear dipole moment $\mathbf{d}^{(N)}(\mathbf{R})=-e\mathbf{R}/6$; while the first term in Eq. (3) vanishes in the case of H_2^+.

The bound-bound transitions can cause resonance effects. Although the matrix elements of bound-free transitions are

small compared to that of electronic transitions, the two-step bound-bound-free transitions via the intermediate discrete state deform the energy and angular distribution of dissociated particles quite a bit and the bound-free matrix elements should be retained.

B. Time-dependent integral equations

To solve the system of coupled Eqs. (3)–(6), we employ the recently developed approach [17,18] based on the properties of TIE. The approach has been successfully applied to the problems of ionization of atoms by multicharged ions and by intense laser fields. Here we present the basic equations, appropriate for the present case.

Since the free-free matrix elements do not directly affect the discrete state amplitudes, $a_{nvK}(t)$, it is possible to neglect them for the evaluation of $a_{nvK}(t)$. The transitions neglected by this approximation are of third order (bound-free-free-bound), actually the role of the free-free transitions was carefully investigated in Ref. [18], and this assumption was confirmed to work well. Neglecting the second term in the right-hand side of Eq. (4) and substituting this into Eq. (3), one obtains

$$i\frac{da_{nvK}(t)}{dt} = \sum_{n',v',K'} \mathbf{U}_{nvK,n'v'K'}(t)a_{n'v'K'}(t)$$
$$+ \int_{t_i}^t \sum_{n',v',K'} \mathbf{W}_{nvK,n'v'K'}(t,\tau)a_{n'v'K'}(\tau)d\tau,$$
(7)

where t_i is the initial time and the kernel $\mathbf{W}_{nvK,n'v'K'}(t,\tau)$ is given by

$$\mathbf{W}_{nvK,n'v'K'}(t,\tau) = -i\int \sum_{n'',K''} \mathbf{U}_{nvK,n''\mathbf{q}K''}(t)$$
$$\times \mathbf{U}_{n''\mathbf{q}K'',n'v'K'}(\tau)d\mathbf{q}.$$
(8)

As we use the orthogonal and normalized unperturbed nuclear wave functions, this can be rewritten as

$$\mathbf{W}_{nvK,n'v'K'}(t,\tau) = -iF(t)F(\tau)\widetilde{\mathbf{W}}_{nvK,n'v'K'}(t-\tau)$$
$$\times \exp[i(E_{nvK}t - E_{n'v'K'}\tau)],$$
(9)

where the new kernel $\widetilde{\mathbf{W}}_{nvK,n'v'K'}(x)$ is given by

$$\widetilde{\mathbf{W}}_{nvK,n'v'K'}(x) = \int \sum_{n'',K''} \langle \theta_{nvK}(\mathbf{R})|\mathbf{d}_{n,n'}^{(e)}(\mathbf{R})$$
$$+ \mathbf{d}^{(N)}(\mathbf{R})|\theta_{n''\mathbf{q}K''}(\mathbf{R})\rangle$$
$$\times \langle \theta_{n''\mathbf{q}K''}(\mathbf{R})|\mathbf{d}_{n,n'}^{(e)}(\mathbf{R})$$
$$+ \mathbf{d}^{(N)}(\mathbf{R})|\theta_{n'v'K'}(\mathbf{R})\rangle e^{i(q^2/2)\cdot x}d\mathbf{q},$$
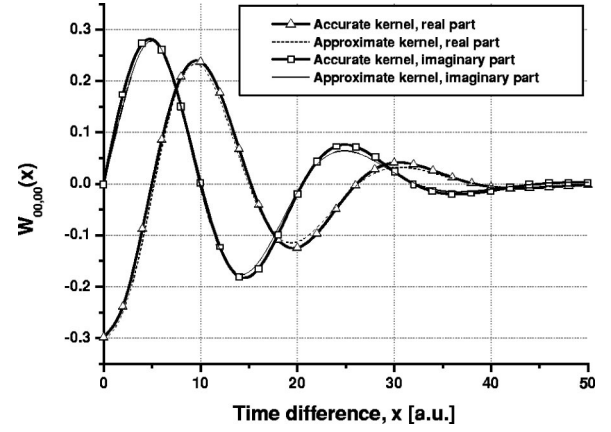(10)

with

FIG. 2. Comparison between real and imaginary parts of the accurate and approximate kernel $\widetilde{\mathbf{W}}_{(1s\sigma_g)00,(1s\sigma_g)00}(t-\tau)$.

$$\widetilde{\mathbf{W}}_{nvK,n'v'K'}(x) = \widetilde{\mathbf{W}}_{nvK,n'v'K'}^*(-x).$$
(11)

The free-free transitions disregarded in Eq. (7) are retained in the evaluation of Eq. (4) for the continuum amplitudes. Putting the solution of Eq. (7) into Eq. (4), we can reduce the problem to the Volterra-type inhomogeneous integral equations with respect to $b_{n\mathbf{q}K}(t)$. The details of this method as well as the generalization of Eq. (7) including the free-free transitions are discussed in Ref. [18]. In the present calculations we do not take into account the free-free transitions, as mentioned above, and solve Eq. (4) without the second term. From the continuum amplitudes, $b_{n\mathbf{q}K}(t)$, we can obtain the photodissociation spectrum by a simple integration.

Since the kernel $\widetilde{\mathbf{W}}_{nvK,n'v'K'}(x)$ defined by Eq. (10) is a function of the molecular parameters only, we can tabulate this and use it repeatedly in any further calculations irrespective of the laser parameters and the initial amplitudes of the discrete states. Equation (7) can be simply solved numerically using the standard algorithms.

The kernel $\widetilde{\mathbf{W}}_{nvK,n'v'K'}(x)$ is a complex function with oscillatory real and imaginary parts, but the absolute value decays monotonically with the argument. One numerical example is shown in Fig. 2, which is for $n=n'=1s\sigma_g$ of H$_2^+$ with $v=v'=0$ and $K=K'=0$. It is possible to represent this kernel $\widetilde{\mathbf{W}}_{nvK,n'v'K'}(x)$ in terms of several simple exponential factors with complex arguments. Figure 2 shows the result of this approximation with the use of five terms. Although the approximation seems to work well, it has been found that the final results of dissociation probability are quite sensitive to the error of this approximation. For instance, in the case of Fig. 2, the final error in dissociation probability is 2% for $I = 10^{13}$ W/cm^2, FWHM = 5 fs, and $\lambda = 100$ nm; while it is 10% for $\lambda = 150$ nm and 400% for $\lambda = 200$ nm.

So we have finally decided not to use this analytical approximations for $\widetilde{\mathbf{W}}_{nvK,n'v'K'}(x)$ in our present calculations.

C. Effects of initial relative phases

In the case of widely distributed initial bound states, the final dissociation probability depends on the initial relative

phases of the coefficients $a_{nvK}(t)$. The initial phase does not play any role, when only one discrete state is initially specified. In the experiments of H_2^+ [9–12], however, the initial condition is given by a wide distribution of target eigenstates and the initial relative phase distribution is, unfortunately, not known. In the present calculations, we have assumed both zero and a uniform distribution of relative phases.

The actual computational scheme is as follows. First, we prepare the time-dependent propagation matrix, $\mathbf{P}_{nvK,n'v'K'}(t)$, for each specified initial state (n',v',K') with unity, i.e., zero phase, initial amplitude assumed. Once this matrix is prepared, the discrete state amplitudes $a_{nvK}(t)$ at time t for any initial condition $a_{n'v'K'}(t_i)$ can be obtained by the simple formula,

$$a_{nvK}(t) = \sum_{n',v',K'} \mathbf{P}_{nvK,n'v'K'}(t) a_{n'v'K'}(t_i). \quad (12)$$

The matrix $\mathbf{P}_{nvK,n'v'K'}(t)$ is not Hermitian and includes the information of the continuum obtained from Eq. (4). The unitarity is, of course, satisfied as

$$\sum_{n,v,K} |a_{nvK}(t)|^2 + \sum_{n,K} \int |b_{n\mathbf{q}K}(t)|^2 d\mathbf{q} = 1. \quad (13)$$

III. H_2^+ CASE

A. Comparison with experiment

First, we have carried out calculations of photodissociation spectra under the laser conditions corresponding to those of Ref. [10]. In this beam experiment, H_2^+ ions were produced in a dc electric discharge ion source, and the dissociation rate was determined directly.

The initial population of rovibrational states of H_2^+ were separately determined in Ref. [10] from the formation process by electron-impact ionization of H_2 [16]. In Fig. 3, the initial populations of H_2^+ ($1s\sigma_g$) used in the present calculations are presented. These are the same as in Ref. [10] except that we do not take into account different rotational state distributions for different vibrational states but used an averaged rotational distribution. The relative phases of initial states are assumed to be equally distributed in the range from 0 to 2π.

In the experiment [10], an intense field was produced by focusing the laser pulses of various pulse energies and lengths to create various intensities. The pulse energy varies from 0.2 mJ to 1.0 mJ and the pulse length from 120 fs to 690 fs. Two wavelengths, 785 nm and 392 nm, were used. In our calculations, we have assumed the Gaussian pulse envelope with FWHM (full width at half maximum) equal to the experimental one.

Comparisons between experimental results [10] and our calculations are presented in Fig. 4. Here, the experimental data are presented in thin line and the present calculations are in thick line. A fairly good agreement is obtained between the two, especially for the positions of main peaks. As the results show, the peak positions and their heights are rather sensitive to the laser parameters.
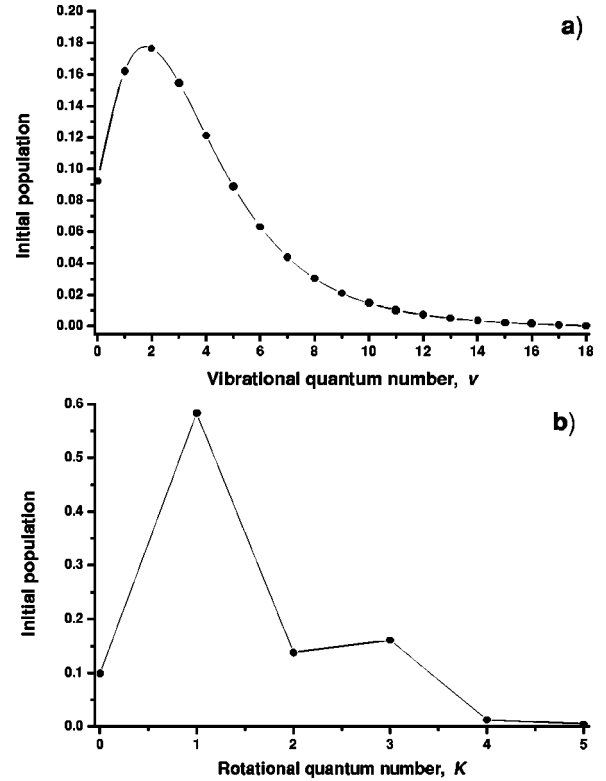

FIG. 3. Initial bound state distribution employed in the calculations: (a) vibrational states, (b) rotational states.

B. Effects of initial phase and population

Since H_2^+ is homonuclear and there is no dipole coupling between the states with different angular-momentum quantum numbers K, the transitions among each manifold of the same angular-momentum can be discussed separately. The total photodissociation spectrum is just the sum of them. Figure 5 presents the energy distributions for different rotational quantum numbers. The bold line represents the total photodissociation spectrum, i.e., the sum of the contributions from $K = 0 \sim 3$, and open circles are the results of one effective rotational quantum number (see the Appendix of Ref. [14]). This effective rotational quantum number was actually taken to be unity in the case of H_2 [14]. The good agreement between the two clearly indicates that one can use only one effective quantum number.

In order to investigate the influence of the uncertainty in the relative phases of initial states, we have carried out the calculations for zero and uniform distribution of them. The results are shown in Fig. 6, which present the photodissociation spectra for the case that all the initial relative phases assumed to be zero (bold line) and for the case of uniform distribution (thin line) for different laser-pulse parameters. The uncertainty in the phases is found to lead to somewhat smoothing of the spectra, depending on the pulse duration. The effect is relatively more significant for short pulses and strong fields. However, for the present purpose of comprehending the overall physics of the processes, it seems to be alright to use the zero relative phases.
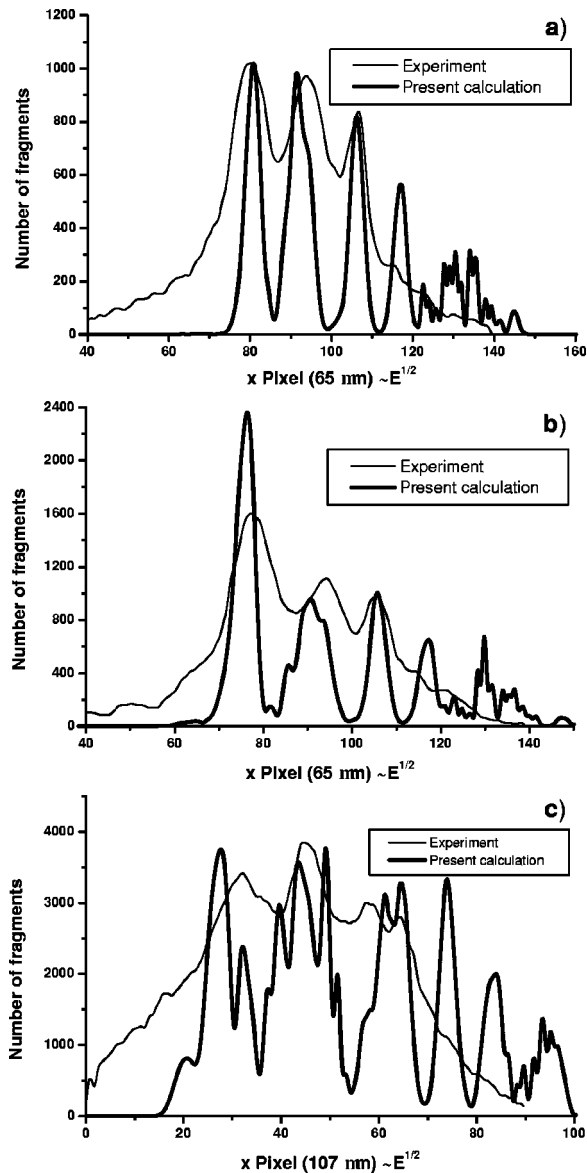
FIG. 4. Comparison of the photodissociation spectrum with the experimental data (Fig. 3 in Ref. [10]) in the case of $H_2{}^+$. Thin line, experimental data. Thick line, present calculation. The wavelength, $\lambda = 785$ nm for all cases. (a) E_{pulse} (energy of the pulse) $= 0.3$ mJ, FWHM (duration) $= 130$ fs, I (intensity) $= 2.5 \times 10^{13}$ W/cm^2; (b) $E_{pulse} = 0.5$ mJ, FWHM $= 130$ fs, $I = 4.2 \times 10^{13}$ W/cm^2; (c) $E_{pulse} = 1.0$ mJ, FWHM $= 130$ fs, $I = 1.5 \times 10^{14}$ W/cm^2.

C. Role of Raman-type transitions.

As was mentioned above, the peak positions and heights of the photodissociation spectra are quite sensitive to the laser intensity. In order to have better understanding of the dependence on the laser intensity, a three-dimensional plot is depicted in Fig. 7 for $\lambda = 785$ nm (1.6 eV).

In the weak-field case ($I \lesssim 2 \cdot 10^{13}$ W/cm^2), in which the simple perturbation theory works [14], one-photon transitions prevail. In this range of intensity, the peak positions, i.e., the energies of dissociated particles (E_{total}), coincide with the sum of the photon energy and the binding energy of
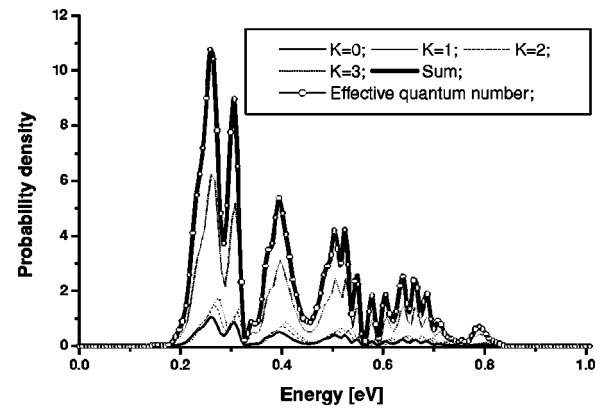

FIG. 5. Energy distributions in the continuum for different rotational numbers, K, in the case of $H_2{}^+$. The bold line presents the total photodissociation spectrum. Open circle, the results with the only effective rotational quantum number $K = 1$ assumed. λ (wavelength) $= 785$ nm, FWHM (duration) $= 65$ fs, I (intensity) $= 3.1 \times 10^{13}$ W/cm^2.

bound states. In accordance with the perturbation theory, the peak heights are proportional to the product of the corresponding bound-state initial population and the Franck-Condon factor. The first factor decays with the vibrational quantum number (Fig. 3), while the second factor grows with the photon energy. As a result, the maximum peak appears for the transition from the $v = 9$ state ($E_{total} = 0.85$ eV).

As the laser intensity grows, multiple transitions naturally play significant roles. Since only the bound-free transitions between $1s\sigma_g$ and $2p\sigma_u$ are possible because of symmetry, significant contribution comes from the Raman-type bound-free-bound transitions. These transitions lead to population increase of lower vibrational states and deforms the spectral profile.

Since an intense laser field causes ac-Stark shifts of bound states and boundary of the continuum, dissociation peaks become wider (this effect is analogous to that in the case of ionization of atoms, see Ref. [22]). The transitions mainly depopulate the levels strongly connected to the continuum. The free-bound transitions also become significant and populate the neighboring levels. In the case of short pulse with wide power spectrum, the effect is enhanced by the resonance transitions due to the higher harmonics. The process leads to the strong one-photon peak corresponding to $v = 9$ ($E_{total} = 0.85$ eV) that goes down with the intensity and the peak corresponding to $v = 8$ ($E_{total} = 0.66$ eV) grows, as seen in Fig. 7.

The mechanism discussed above is clearly illustrated in Fig. 8, which depicts the time variation of each vibrational level population. The populations of $v \leqslant 8$ do not decrease monotonically, but locally grow in certain time intervals (in the case of $v \leqslant 7$, the population even exceeds the initial one). For instance, the $v = 7$ population grows significantly in the time interval $30 \sim 50$ fs. Even in the case of $v = 8$, the population increases at around 50 fs. The higher vibrational states, on the other hand, depopulate. Eventually, all these populations decrease and the continuum population steadily increases.
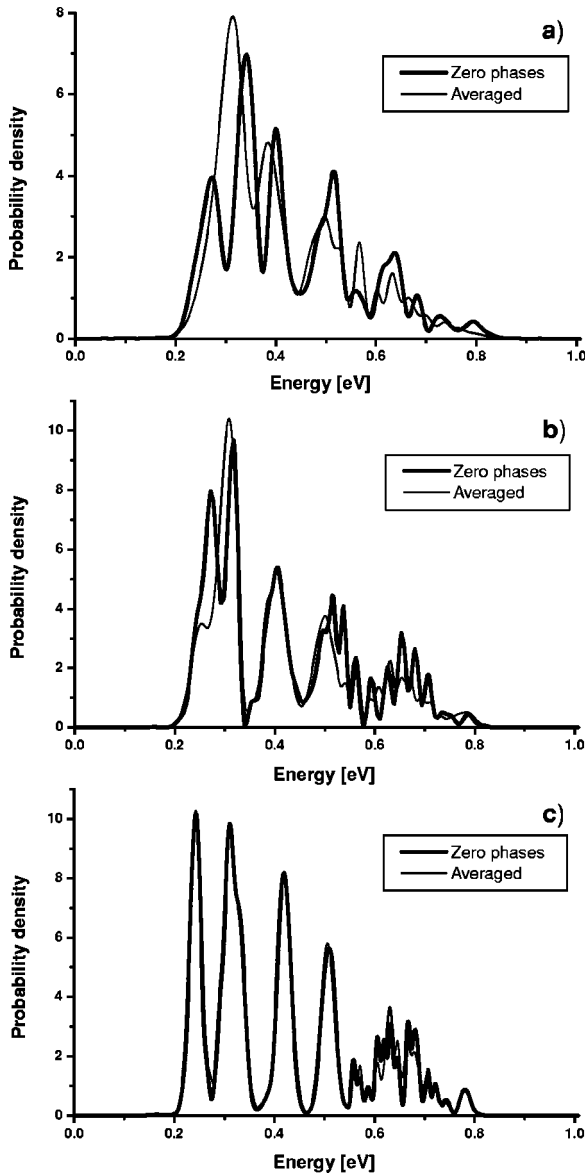
FIG. 6. Comparison of photodissociation spectra of H_2^+ between the case that all the initial relative phases are assumed to be zero (thick line) and the case of uniform distribution (thin line). $\lambda = 785$ nm for all cases: (a) FWHM $= 40$ fs, $I = 2.5 \times 10^{13}$ W/cm^2; (b) FWHM $= 65$ fs, $I = 2.5 \times 10^{13}$ W/cm^2; (c) FWHM $= 130$ fs, $I = 2.5 \times 10^{13}$ W/cm^2.

Recently, the enhancement of photodissociation rate of relatively low vibrational states ($v = 6, 7$) was explained [10] by the bond softening effect [3,4]. The present close-coupling calculations suggest that this phenomenon is not just due to the bond softening effect, but the Raman type transitions also contribute.

Besides, the processes discussed above, i.e., the step-by-step multiphoton dissociation (above threshold dissociation [1,2]) are also confirmed to contribute significantly. This plays a major role in the high-energy region of the spectrum. Peaks at energies above $E_{total} = 1.6$ eV in Fig. 7 are explained by this mechanism.
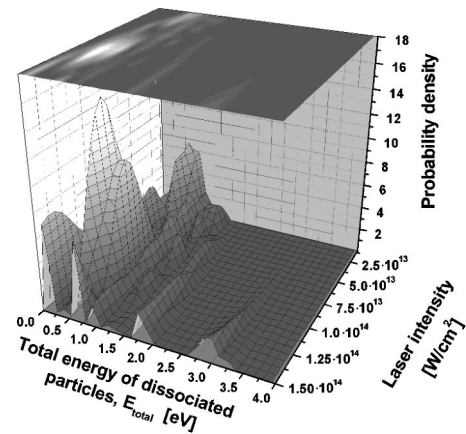

FIG. 7. Three-dimensional plot of photodissociation spectra of H_2^+ as a function of field intensity. $\lambda = 785$ nm, FWHM $= 40$ fs.

IV. HD$^+$ CASE

A. Role of bound-bound transitions.

Since there is no experiment available yet for HD$^+$ and it is interesting to compare with H_2^+ case under the same condition, we have assumed the same initial conditions as before (see Fig. 3).

The reduced mass ratio of HD$^+$ and H_2^+ is 4/3 and the bound-free matrix elements of electronic-dipole transition are not very different. The main difference in the dissociation process is expected to come from the nuclear dipole transitions in HD$^+$.

Figure 9 presents the energy distributions of the dissociated fragments for different angular-momentum quantum numbers K. Our calculations show that the dissociation continuum of the $1s\sigma_g$ state contributes much less than that of $2p\sigma_u$ state for any pulse parameters, and the difference in the dissociation spectra and angular distribution can be explained only in terms of the transitions via intermediate bound states. This means that the energy and angular distributions should be sensitive to the laser frequency [18].

Figure 10 shows a comparison of the dissociation spectra with and without the contributions from the bound-bound transitions. One can easily notice that the new type of transitions produce new peaks at energies that cannot be reached
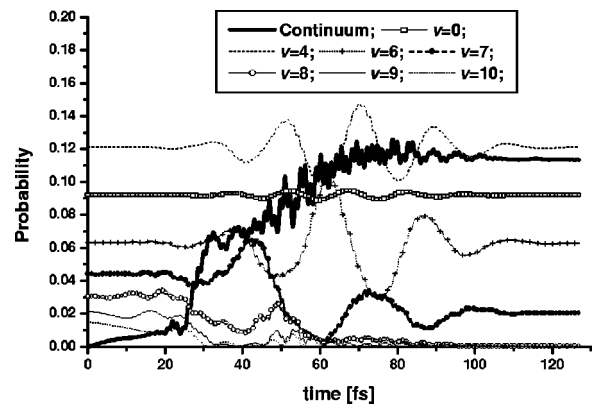

FIG. 8. Time variation of vibrational states populations in the case of H_2^+ $I = 3.1 \cdot 10^{13}$ W/cm^2; $\lambda = 785$ nm; FWHM $= 40$ fs.
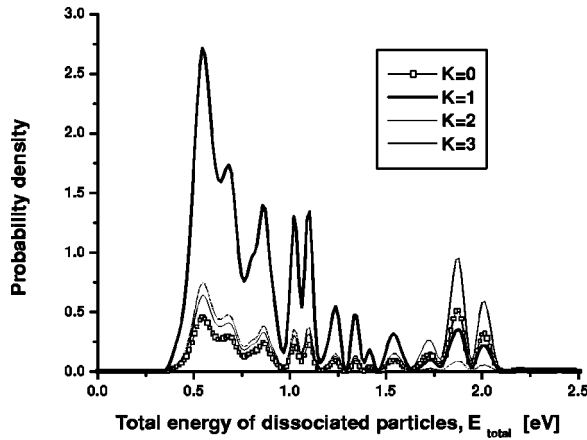
FIG. 9. Dissociation spectrum for different rotational numbers, K in the case of HD$^+$. $\lambda = 785$ nm, FWHM$= 65$ fs, $I = 3.1 \cdot 10^{13}$ W/cm^2.

FIG. 11. HD$^+$ case. Photodissociation spectra as a function of field intensity. $\lambda = 785$ nm; FWHM$= 40$ fs.

by the direct electronic-dipole transitions. Particles with such energies have different angular-momentum quantum numbers and angular distributions. The peaks at energies $\lesssim 1.4$ eV are mainly produced by one-photon electronic-dipole transition from the states with $v = 7 \sim 9$, as was discussed before. The effects of Raman-type transitions discussed in the preceding section play roles in the dissociation spectrum in this low-energy region.

The additional structure at higher energies is due to the two-step transitions from deeper bound states. These highly populated states have no possibilities to dissociate by not only one- but also two-photon direct transitions because of the small Franck-Condon factors in that energy region. The one-photon nuclear dipole bound-bound transitions first populate higher bound states and the next one-photon electronic-dipole transition leads to the peaks in this energy region. The corresponding Franck-Condon factors between the high bound states and the continuum are big enough.

B. Dissociation spectra and angular distributions as a function of pulse parameters

Figure 11 presents photodissociation spectrum as a function of laser intensity. In the low intensity region, the direct
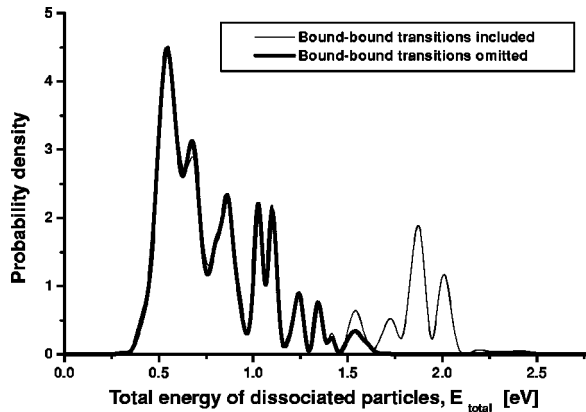
electronic-dipole transitions prevail and the peak structures discussed above can be observed. When the intensity increases, two types of competing processes determine the spectral profile. The first one is the same as that discussed in Sec. III and mainly determines the spectral profile at low energies. The second type of processes are the two-step transitions from deep bound states discussed in the preceding section. At high intensities, the latter processes become significant.

The frequency dependence of the spectra is presented in Fig. 12. At low frequencies up to one half of the dissociation energy of the lowest state, the multistep bound-bound transitions play important roles. The frequency dependence is complicated in this region. At higher frequencies (1.3 eV), two distinct sets of peaks corresponding to the first and second types of processes coexists. When the frequency exceeds 2.6 eV, the one-photon bound-bound transitions are not possible and the high-energy set of peaks can be explained as the two-photon nuclear dipole bound-free transitions. The probability of such transitions is smaller than the two-photon transitions via intermediate discrete state and the corresponding peaks become lower.

FIG. 10. Comparison of the dissociation spectra of HD$^+$ case with (thin line) and without (thick line) bound-bound transitions. Parameters are the same as in Fig. 9
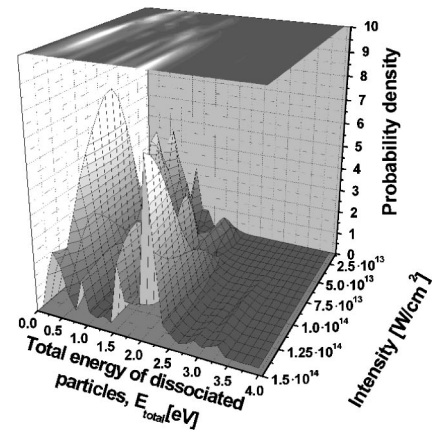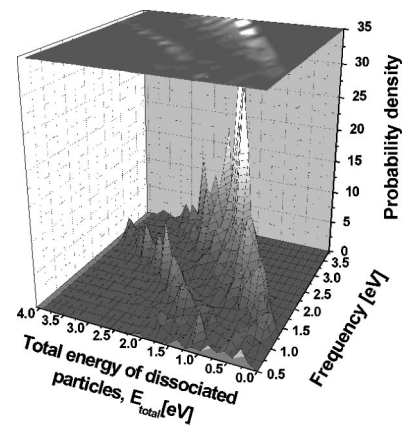

FIG. 12. 3D plot of photodissociation spectra of HD$^+$ as a function of field frequency. $I = 8 \times 10^{13}$ W/cm^2; FWHM$= 40$ fs.

The competition between the direct electronic-dipole transitions and the two-step transitions via intermediate discrete states determines also the angular distributions. Considering the fact that a uniform distribution is assumed for the initial relative phases and cross terms between different continuum amplitudes are confirmed to be negligibly small, we can simplify the expression of angular distribution as

$$P\left(\frac{\mathbf{q}}{q}\right) = \sum_{n,K} \int |b_{n\mathbf{q}K}(\infty)|^2 q^2 dq. \qquad (14)$$

At low intensities, the angular distribution is mainly determined by the initial population of discrete states with different rotational quantum numbers. Since $K=1$ is the dominant component, the angular distribution is close to $\cos^2$. As the intensity increases, the nuclear dipole transitions significantly change the population of continuum with different rotational quantum numbers and so the angular distribution. In a wide range of intensity, $6 \cdot 10^{13} \sim 1.2 \cdot 10^{14}$ W/cm^2, it becomes closer to $\cos^4$. At higher intensities, it becomes more complicated.

V. CONCLUSIONS

The photodissociation of $H_2{}^+$ and HD^+ by an intense laser pulse is investigated by solving the close-coupling equations without discretization.

For the case of $H_2{}^+$, the photodissociation spectra has been calculated under the condition mimicking the experimental one and a fairly good agreement with the experiment has been obtained.

The multistep transitions have been found to play significant roles in the photodissociation processes in an intense laser field. In the case of homonuclear $H_2{}^+$, only direct bound-free electronic-dipole transitions are possible. In this case, the Raman-type transitions via intermediate dissociation continuum lead to temporal population increase of lower vibrational states and thus, finally, deforms the spectral profile. This effect has been found to be crucial to explain the experiment and the bond softening cannot be good enough.

In the case of heteronuclear HD^+, the additional sequential transitions via intermediate bound states play crucial roles. The two types of multistep transitions mentioned above lead to energetically well separated structures in the dissociation spectra. The competition between the direct electronic-dipole transitions and the two-step transitions via intermediate discrete states determines also the angular distribution.

The uncertainty in the initial relative phases has been found to lead to somewhat smoothing of the spectra, depending on the pulse length.

The calculated results of photodissociation spectra have been presented in three-dimensional plot by introducing the field intensity or frequency as an extra axis. This is helpful for clearly understanding the dependence of photodissociation dynamics on the laser parameters.

[1] A. Giusti-Suzor, X. He, and O. Atabek, Phys. Rev. Lett. **64**, 515 (1990).

[2] A. Bandrauk and J. Gauthier, J. Opt. Soc. Am. B **7**, 1422 (1990).

[3] *Molecule in Intense Laser Fields*, edited by A. Bandrauk (Marcel Dekker, New York, 1995).

[4] P. Bucksbaum, A. Zavriyev, H. Muller, and D. Schumacher, Phys. Rev. Lett. **64**, 1883 (1990).

[5] G. Yao and S.-I. Chu, Phys. Rev. A **48**, 485 (1993).

[6] L. Frasinski, J. Posthumus, J. Plumridge, E. Charron, and B. Yang, Phys. Rev. Lett. **83**, 3625 (1999).

[7] E. Charron, A. Giusti-Suzor, and F. H. Mies, Phys. Rev. Lett. **75**, 2815 (1995).

[8] S. Sen, S. Ghosh, S. S. Bhattacharyya, and S. Saha, J. Chem. Phys. **116**, 1286 (2002).

[9] G. N. Gibson, M. Li, C. Guo, and J. Neira, Phys. Rev. Lett. **79**, 2022 (1997).

[10] K. Sändig, H. Figger, and T. W. Hänsch, Phys. Rev. Lett. **85**, 4876 (2000).

[11] I. Williams *et al.*, J. Phys. B **33**, 2743 (2000).

[12] W. A. Bryan, A. A. A. El-Zein, T. R. J. Goodworth, W. R. Newell, I. D. Williams, P. McKenna, I. M. G. Johnston, P. F. Taday, and A. J. Langley, in *Proceedings of the 22nd International Conference on the Physics of Electronic and Atomic Collisions*, edited by S. Datz, M. E. Bannister, H. F. Krause, L. H. Saddiq, D. R. Shultz, and C. R. Vane (Rinton Press, Santa Fe, 2001).

[13] A. Giusti-Suzor, F. H. Mies, L. F. DiMauro, E. Charron, and B. Yang, J. Phys. B **28**, 309 (1995).

[14] F. von Busch and G. Dunn, Phys. Rev. A **5**, 1726 (1972).

[15] D. P. D. Bruijn, J. Neuteboom, and J. Los, Chem. Phys. **85**, 233 (1984).

[16] W. Koot, W. V. D. Zanda, and D. D. Bruijn, Chem. Phys. **115**, 297 (1987).

[17] A. Kondorskiy and L. Presnyakov, J. Phys. B **34**, L663 (2001).

[18] A. Kondorskiy and L. Presnyakov, Laser Phys. **12**, 449 (2002).

[19] H. Wind, J. Chem. Phys. **43**, 2956 (1965).

[20] F. V. Bunkin and I. I. Tugov, Phys. Rev. A **8**, 601 (1973).

[21] D. R. Bates, J. Chem. Phys. **19**, 1122 (1951).

[22] L. F. DiMauro and P. Agostini, Adv. At., Mol., Opt. Phys. **35**, 79 (1995).